THE JOURNAL OF PHYSICAL CHEMISTRY B

Article

pubs.acs.org/JPCB

# Dynamics of the Chiral Liquid Crystal 4′-Butyl-4-(*S*)-(2-methylbutoxy)azoxybenzene in the Isotropic, Cholesteric, and Solid Phases: A Fast Field-Cycling NMR Relaxometry Study

Elisa Carignani,[#] Lucia Calucci,*[,#] Ewa Juszyńska-Gałązka,[§] Mirosław Gałązka,[§] Maria Massalska-Arodź,[§] Claudia Forte,[#] and Marco Geppi*[,‡,#]

[#]Consiglio Nazionale delle Ricerche − CNR, Istituto di Chimica dei Composti OrganoMetallici, via G. Moruzzi 1, 56124 Pisa, Italy

[§]The Henryk Niewodniczański Institute of Nuclear Physics, Polish Academy of Sciences, E. Radzikowskiego 152, 31-342 Krakow, Poland

[‡]Dipartimento di Chimica e Chimica Industriale, Università di Pisa, via G. Moruzzi 13, 56124 Pisa, Italy

Supporting Information

**ABSTRACT:** $^1$H NMR relaxometry was applied to investigate dynamic processes in the isotropic liquid, cholesteric, and crystalline phases of the chiral mesogen 4′-butyl-4-(*S*)-(2-methylbutoxy)azoxybenzene (4ABO5*). To this aim, $^1$H longitudinal relaxation rates were measured as a function of temperature (between 257 and 319 K) and Larmor frequency (from 10 kHz to 35 MHz by a fast field-cycling relaxometer and at 400 MHz by an NMR spectrometer). The NMR relaxation dispersion (NMRD) curves so obtained were analyzed in terms of models suitable for the description of dynamic processes in the different phases, thus quantitatively determining values of characteristic motional parameters. In particular, internal and overall rotations/reorientations, molecular translational diffusion, and collective motions contribute to relaxation in the isotropic and cholesteric phases, whereas, in the crystalline phase, relaxation is mainly determined by internal motions and molecular reorientations. The results were discussed and compared with those previously obtained on the same compound by dielectric relaxation spectroscopy.

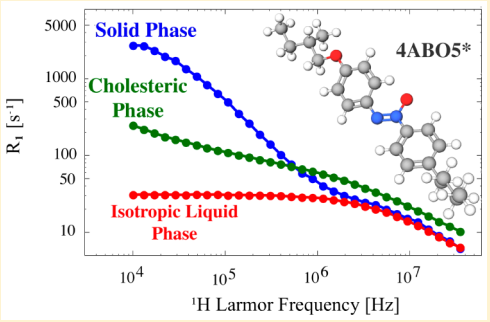


## INTRODUCTION

Liquid crystals, simultaneously exhibiting properties peculiar to solid and liquid phases, are especially interesting for both basic research and technological applications.[1−4] In particular, chiral compounds forming a cholesteric phase have raised much interest for their electro-optical applications, such as LCD displays and self-assembled microlasers.

The rich polymorphism of liquid crystalline materials, which, besides the isotropic liquid (I) and solid crystalline (Cr) phases, may include several mesophases with different degrees of orientational and positional order (i.e., for calamitic liquid crystals, nematic (N), cholesteric or chiral nematic (N*), smectic (Sm) phases), is strongly related to the motional degrees of freedom of the molecules in the different phases. Therefore, a thorough investigation of dynamic processes is deemed to be fundamental for understanding liquid crystal polymorphism and, consequently, for designing novel materials with useful applicative properties.

The complex dynamics of liquid crystals is characterized by a superposition of internal (rotations or jumps of molecular fragments), molecular (rotations of the molecule around the long and short axes, and translational diffusion), and collective motions (i.e., orientational fluctuations of the phase director with respect to its time-averaged orientation, indicated as order fluctuations of the director (ODF) in the nematic phase and as layer undulations in liquid-like smectic phases), which occur over different time scales. In particular, internal, reorientational, and translational motions are usually characterized by short correlation times ($10^{-12}$ to $10^{-8}$ s), whereas collective motions are characterized by a distribution of fluctuation modes with amplitudes and damping times determined by the anisotropic viscoelastic properties of the liquid crystal.[5−7] Among the methods employed to study dynamics in condensed phases, nuclear magnetic resonance (NMR) relaxometry and broad-band dielectric spectroscopy (BDS) are the most powerful ones, both yielding a detailed characterization of motions over a wide frequency range.[5−13]

In the last decades, field-cycling relaxometry experiments, which allow frequency-dependent measurements of $^1$H longitudinal relaxation times ($T_1$) to be performed over the kilohertz to tens of megahertz frequency range (10 kHz to 40 MHz using commercial fast field-cycling (FFC) relaxometers, while frequencies even below 100 Hz can be reached with homemade relaxometers where earth field is compensated),[11,14−17] were successfully applied to get insights into the dynamics in liquid crystalline materials, also in combination

**Received:** April 13, 2016
**Revised:** May 16, 2016
**Published:** May 17, 2016





DOI: 10.1021/acs.jpcb.6b03773
*J. Phys. Chem. B* 2016, 120, 5083−5092

with $^1$H $T_1$ measurements at higher frequencies (≥60 MHz) by NMR spectrometers. Mesogenic materials of increasing complexity, from conventional calamitic phases to chiral smectic phases, frustrated phases, banana mesophases, and dendrimeric liquid crystals, were investigated.[7,11−13,18−21] Moreover, $^1$H relaxometry was applied to investigate the pretransitional formation of ordered molecular clusters of mesogenic molecules in the isotropic phase and to study the motional restrictions for spatially confined liquid crystals.[22]

Proton spin−lattice relaxation is determined by the modulation, due to reorientational and translational motions, of intra- and intermolecular homonuclear dipolar interactions between protons.[23] $^1$H NMR relaxometry can indeed be applied to study internal motions (IM), molecular rotations/reorientations (MR), and translational self-diffusion (SD), giving contributions to relaxation at the highest frequencies.[5,11−13,18] Collective motions (ODF) present in fluid mesophases may also strongly contribute to $^1$H relaxation in the low frequency region (below $10^5$ Hz), where they give peculiar frequency dependences.[11,24,25] Local order fluctuations (OF) associated with the onset and decay of weakly ordered molecular clusters, connected with pretransitional effects, were also found to affect $^1$H relaxation in the isotropic liquid phase of mesogens upon approaching the transition to the nematic phase.[19] For the cholesteric mesophase, characterized by a helical twist of the nematic director, molecular rotations induced by translational diffusion along the helical axis (RMTD) have also been found to contribute to relaxation at low frequencies.[19−21,26] Theoretical models have been developed by different research groups, suitable to describe the effects of the different motions on proton longitudinal relaxation and, therefore, necessary to obtain quantitative dynamic information from relaxation rate ($R_1 = 1/T_1$) dispersions (NMRD) arising from NMR relaxometry experiments.[5−7,12]

BDS has also been successfully applied for the investigation of molecular dynamics in liquid crystalline materials,[3,10] the dielectric response being due to correlation functions of the polarization fluctuations induced by motions of polar molecules. Except for the conductivity process present in the low-frequency region (<$10^4$ Hz), two main relaxation processes are generally found in dielectric spectra by BDS, which are attributed to reorientations of the molecules around their short (flip-flop motion with frequencies in the MHz range) and long axes (at higher frequencies), both inducing reorientations of the molecular dipoles.[5,27]

In a recent work,[28] BDS was applied by some of us to investigate the dynamics of the chiral calamitic mesogen 4′-butyl-4-(*S*)-(2-methylbutoxy)azoxybenzene (4ABO5* in Figure 1) in the I, N*, and Cr phases over a broad frequency range (mHz − GHz). Three relaxation processes—molecular reorientations (in all phases) and collective motions (in the Cr and N* phases)—were singled out and quantitatively characterized. The slowest relaxation process, ascribed to collective motions, was observed in the low frequency region (below $10^2$ and $10^3$ Hz in the Cr and N* phases, respectively). The intermediate and fastest relaxation processes, ascribed to reorientational motions around the short (S motion) and long (L motion) molecular axes, respectively, gave contributions to dielectric relaxation in different frequency ranges depending on the phase.

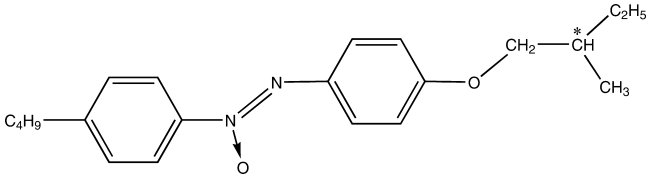


**Figure 1.** Molecular structure of 4′-butyl-4-(*S*)-(2-methylbutoxy)-azoxybenzene (4ABO5*).

In the present work, the dynamics of 4ABO5* was investigated by means of $^1$H NMR relaxometry. Dynamic processes encompassing the kHz to hundreds of MHz frequency scale, including internal, molecular, and collective motions, were highlighted and quantitatively characterized on the basis of suitable models. The results obtained were also compared to those previously found by BDS experiments; in particular, for the Cr phase, where both NMR relaxometry and dielectric spectroscopy data were interpreted on the basis of the same motional model, a scaling procedure was applied to directly compare the $^1$H NMR relaxation rate to the imaginary part of the dielectric susceptibility.

## EXPERIMENTAL SECTION

**Materials.** 4′-Butyl-4-(*S*)-(2-methylbutoxy)azoxybenzene (4ABO5*) was synthesized by the group of Prof. Dąbrowski at the Military University of Technology, Warsaw (Poland). The phase transition temperatures of 4ABO5*, determined by Differential Scanning Calorimetry (DSC) in previous studies,[28,29] are the following: Cr-(285.26 K)-N*-(299.65 K)-I (on heating) and I-(298.82 K)-N*-(277.66 K)-Cr (on cooling).

**FFC NMR Relaxometry Measurements.** $^1$H NMRD profiles were obtained by measuring longitudinal relaxation times at 32 different Larmor frequency values in the range between 10 kHz and 35 MHz using a SpinMaster FFC-2000 (Stelar srl) relaxometer. The sample was contained in a standard 10 mm NMR tube. The nonprepolarized (NP) and prepolarized (PP) sequences[30] were used for measurements at high (≥12 MHz) and low (≤12 MHz) fields, respectively. The polarizing ($B_{pol}$) and detection ($B_{acq}$) fields were 0.70 and 0.50 T, corresponding to $^1$H Larmor frequencies of 30.0 and 21.5 MHz, respectively, with a switching time of 3 ms. The 90° pulse duration was 11 $\mu$s and a single scan was acquired. All the other experimental parameters were optimized for each experiment. Each longitudinal relaxation trend was acquired with at least 16 values of the variable delay $t$ and was then fitted to eq 1:

$$M(t) = M_{relax} + (M_{pol} - M_{relax})\exp(-t/T_1) \quad (1)$$

using the SpinMaster integrated fitting procedure. In eq 1, $M_{pol}$ and $M_{relax}$ are the magnetization values in the polarizing and relaxation fields, respectively; $M_{pol} = 0$ for the NP experiments. In all cases, monoexponential functions well reproduced the experimental trends, with errors on $R_1$ values lower than 3%.

The NMRD profiles were acquired every 1 or 2 K on slow cooling from the isotropic phase in the temperature range between 319 and 257 K. The temperature was controlled within ±0.1 K with a Stelar VTC90 variable temperature controller and was stabilized for at least 10 min before each measurement.

**$^1$H $T_1$ Measurements at 400 MHz.** $^1$H $T_1$ values were measured at a Larmor frequency of 400.35 MHz using an Infinity Plus 400 spectrometer (Agilent) equipped with a static goniometric probe. The Inversion Recovery and Saturation



DOI: 10.1021/acs.jpcb.6b03773
J. Phys. Chem. B 2016, 120, 5083−5092

Recovery pulse sequences were employed in the I phase and in the N* and Cr phases, respectively. The 90° pulse duration was 4.5 $\mu$s, and the recycle delay was 5 s; 4 scans were acquired. The experiments were performed every 1 or 2 K on slow cooling from the isotropic phase in the temperature range between 319 and 257 K. The temperature was controlled within ±0.3 K and was stabilized for at least 10 min before each measurement. In all cases, a monoexponential function well-reproduced the experimental magnetization trend, with errors on $R_1$ values lower than 1%.

**NMRD Profile Analysis.** The analysis of the experimental $^1$H NMRD profiles in terms of models for longitudinal relaxation in the presence of different dynamic processes was performed using the least-squares minimization procedure implemented in the Fitteia environment[31,32] for I and N* phases, whereas a software purposely written in Mathematica[33] environment was used for the Cr phase.

## THEORETICAL BACKGROUND

**Models for the Analysis of $^1$H Longitudinal Relaxation.** Experimental $R_1$ values are considered as a sum of contributions ($R_1^i$) coming from different relaxation mechanisms, all depending on both temperature and angular Larmor frequency ($\omega = 2\pi\nu$) through spectral densities of motions.[23,34] It is generally assumed that these contributions are statistically independent and/or have distinct characteristic time scales, and therefore any cross-relaxation contribution is considered negligible.

In the isotropic liquid phase, contributions to $R_1$ arising from rotational internal ($R_1^{IM}$) and overall molecular ($R_1^{MR}$) motions and translational self-diffusion ($R_1^{SD}$) can be present. In this phase, the dependence of the $R_1^{IM}$ and $R_1^{MR}$ relaxation rates on the Larmor frequency are commonly expressed using the Blombergen-Purcell-Pound (BPP) model:[35]

$$R_1^i = C_i[J(\omega) + 4J(2\omega)] \tag{2}$$

where $C_i$ is a relaxation amplitude factor depending on the strength of the homonuclear dipolar interaction and the spectral density $J(\omega)$ depends on the correlation time of motion $\tau$ according to the following equation:

$$J^{BPP}(\omega) = \frac{2\tau}{1 + (\omega\tau)^2} \tag{3}$$

On the other hand, the translational self-diffusion contribution to proton spin−lattice relaxation, $R_1^{SD}$, can be calculated analytically using the Torrey model,[36] which depends on the spin density, the self-diffusion coefficient, the mean square jump distance and the width of the molecule. In the low-frequency region a dependence of $R_1^{SD}$ on the square root of the Larmor frequency is expected.[36−39] In addition, a contribution to $R_1$ due to local order fluctuations (OF) could be present upon approaching the transition to the N* phase. This contribution can be expressed as follows:[19]

$$R_1^{OF} = \frac{C_{OF}}{\sqrt{\omega}} \int_{\omega_{OFmin}/\omega}^{\omega_{OFmax}/\omega} \frac{\sqrt{x}}{1 + (x + \omega_0/\omega)^2} dx \tag{4}$$

where $\omega_{OFmin}$ and $\omega_{OFmax}$ are the low and high cutoff frequencies, and $\omega_0$, which depends on the size of partially ordered molecular clusters present in the isotropic phase, also acts as a cutoff frequency; $C_{OF}$ is a coefficient which depends on temperature, elastic, and viscosity properties of the mesophase, as well as on the interproton distance. Eq 4 predicts a dependence of $R_1^{OF}$ on the inverse square root of the Larmor frequency over a range determined by the cutoff frequency values.

In liquid crystalline phases, overall rotational/reorientational motions are typically described by diffusional models considering their anisotropic character;[5−7,12,13] for instance, the Woessner model has been adopted to express $R_1^{MR}$ contributions in the analysis of NMRD curves acquired by FFC NMR.[40,41] These models, however, require the knowledge of geometrical and orientational order parameters, which are not always available. Moreover, the relaxation rates measured are often not relative to single well-distinguished proton pairs nor to a uniformly oriented sample, but rather, they are relative to an average over different proton pairs and orientations. Therefore, in the case of complex anisotropic molecules, molecular reorientations can be described, to a first approximation, by a sum of BPP relaxation equations with different characteristic correlation times.[20,21] BPP relaxation equations are also generally employed for the $R_1^{IM}$ contribution. For the relaxation rate contribution associated with translational diffusion ($R_1^{SD}$) in liquid crystalline phases, variants of the Torrey model, which take into account the anisotropy of the self-diffusion, have been developed by Zumer and Vilfan.[38,42] Moreover, as anticipated, order director fluctuations may strongly contribute to relaxation at low frequencies. In particular, in the N and N* phases, the $R_1^{ODF}$ contribution depends on the inverse of the square root of the Larmor frequency, as predicted by the Pincus theory,[43] and can be written in the form:[19,44]

$$R_1^{ODF} = \frac{C_{ODF}}{\sqrt{\omega}}\left[g_N\left(\frac{\omega_{ODFmax}}{\omega}\right) - g_N\left(\frac{\omega_{ODFmin}}{\omega}\right)\right] \tag{5}$$

where $C_{ODF}$ is a factor depending on the absolute temperature, the principal molecular order parameter, and macroscopic parameters, such as the Frank elastic constant and viscosity coefficient, as well as on interproton distances. In eq 5, $\omega_{ODFmax}$ and $\omega_{ODFmin}$ are the high and low frequency cut-offs, respectively, and the $g_N$ function is

$$g_N(x) = \frac{1}{\pi}\left[\arctan(\sqrt{2x} + 1) + \arctan(\sqrt{2x} - 1) - \operatorname{arctanh}\left(\frac{\sqrt{2x}}{1 + x}\right)\right] \tag{6}$$

Finally, a contribution due to RMTD, associated with the molecular diffusion along the helical axis of the N* phase, has been reported and modeled by Vilfan et al.[26]

In solid phases, self-diffusion and collective motions are absent or extremely slow, and they can be neglected in the analysis of proton longitudinal relaxation. Therefore, only the internal motions and, in some cases, molecular reorientations should be taken into account in NMRD analyses. Moreover, the BPP model, which implies a completely random process described by a single correlation time,[35] is usually not suitable to express spectral densities in solids. In fact, motions may be inherently nonrandom, which might be the case if they are correlated; second, within an ensemble of reorienting units (i.e., the whole sample), there may be subensembles, each of which involves units undergoing a random motion characterized by a different correlation time.[6,45] A model often used in solid phases to express the spectral density to be inserted in eq 2 is the phenomenological Havriliak−Negami (HN) model,[46] which takes into account the presence of both a distribution of correlation times, corresponding to a distribution of



DOI: 10.1021/acs.jpcb.6b03773
J. Phys. Chem. B 2016, 120, 5083−5092

motional energy barriers, and correlation between motions. According to the HN model, the spectral density has the following form:

$$J^{HN}(\omega) = \frac{2}{\omega}\sin\left[\beta \tan^{-1}\left(\frac{(\omega\tau)^{\delta}\sin\left(\frac{\delta\pi}{2}\right)}{1 + (\omega\tau)^{\delta}\cos\left(\frac{\delta\pi}{2}\right)}\right)\right] \left[1 + (\omega\tau)^{2\delta} + 2(\omega\tau)^{\delta}\cos\left(\frac{\delta\pi}{2}\right)\right]^{-\beta/2} \quad (7)$$

where $\delta$, ranging from 0 to 1, is a measure of the correlation of the motions ($\delta = 0$ corresponding to perfect correlation) and $\delta\beta$, also ranging from 0 to 1, is a measure of the spread in energy barriers (with $\delta\beta = 0$ corresponding to the broadest allowed distribution). It is worth noting that this expression reduces to the Cole−Cole spectral density for $\beta = 1$, to the Cole−Davidson spectral density for $\delta = 1$, and to the BPP spectral density for $\beta = \delta = 1$.[45]

**Relationship between NMR Relaxometry and Dielectric Spectroscopy.** The imaginary part of the normalized electric susceptibility obtained by BDS experiments can be expressed as a function of the spectral density as[47]

$$\chi''_{BDS}(\omega) = \omega J(\omega) \quad (8)$$

Different models are used in dielectric spectroscopy studies to express the spectral density and, therefore, to extract correlation times of motions from the analysis of experimental data; the most employed are empirical functions derived by a generalization of the simple BPP function (usually referred to as Debye function in dielectric spectroscopy), such as the Havriliak−Negami, Cole−Davidson, and Cole−Cole expressions (eq 7).[45,46,48]

The relationship between susceptibility and spectral density can be used to establish analogies between BDS and $^1$H NMR relaxometry by converting the NMRD data to a susceptibility representation.[49,50]

$$\chi''_{NMR} = \omega R_1(\omega) = K[\omega J(\omega) + 4\omega J(2\omega)] = K[\chi''(\omega) + 2\chi''(2\omega)] \quad (9)$$

This representation allows a more straightforward comparison of BDS and $^1$H FFC NMR data to be performed, as shown in the literature for several viscous liquids and polymer melts.[14,15,51] In this regard, the frequency−temperature superposition (FTS), which assumes that the spectral shape of the susceptibility function does not change with temperature, is usually exploited in the analysis.[48,49] Considering the FTS, a master curve spanning several frequency decades is built for the electric and NMR susceptibilities by appropriately shifting the $\chi''_{BDS}(\omega)$ or $\chi''_{NMR}$ curves acquired at different temperatures along the frequency axis; the resulting master curve is plotted vs $\omega\tau$, $\tau(T)$ being, at each temperature, the time constant characteristic for the motion under examination. For curves which clearly exhibit a maximum at a frequency $\omega_{max}$, $\tau(T)$ can be determined considering that $\omega_{max}\tau(T) = 1$; for curves where a maximum is not clearly detected, $\tau(T)$ can be extracted from the shift factor. A more accurate determination of the time constant may be obtained by fitting the experimental data to suitable model functions. In that case, a model-dependent average correlation time ($\tau^{av}(T)$) is extracted; for the Debye model, $\tau^{av}(T)$ coincides with $\tau(T)$, whereas for Havriliak−Negami, Cole−Davidson, and Cole−Cole models, it is proportional to it through characteristic coefficients. For instance $\tau^{av}(T) = \beta\tau(T)$ for the Cole−Davidson model.[14,15,48−51] Moreover, several important factors must be considered when comparing BDS and NMR data, also depending on the investigated motions and physical state of materials.[23,45] First, in BDS, relaxation is determined by the modulation of rank-one interactions, whereas homonuclear dipole−dipole interactions modulated by motions inducing $^1$H longitudinal relaxation are of rank-two. Second, different motions might be involved in BDS and NMR relaxation, the two techniques being sensitive to reorientations of different vectors. In particular, for $^1$H longitudinal relaxation the contribution of the modulation of the intermolecular dipolar interactions by translational motions cannot be excluded, although the intramolecular contribution is usually dominant due to the short-range nature of the dipolar interaction. In liquid crystalline phases, the presence of collective motions strongly affects $^1$H NMR relaxation at low frequency, sometimes hampering an unambiguous distinction among the different possible contributions of molecular motions. Finally, spin diffusion affects $^1$H longitudinal relaxation, whereas there is no analogous phenomenon in dielectric relaxation.

## RESULTS AND DISCUSSION

**Trends of $^1$H Relaxation Rate with Frequency and Temperature.** $^1$H longitudinal relaxation times, $T_1$, were measured at Larmor frequencies from 10 kHz to 35 MHz using a FFC NMR relaxometer and at 400 MHz using an NMR spectrometer in the temperature range between 257 and 319 K, on cooling from the isotropic phase. The strength of the magnetic fields used in our experiments was not large enough to uniformly align the long axes of the mesogenic molecules throughout the sample. In spite of this, in all cases a single exponential function satisfactorily reproduced the magnetization trends, so that a single $T_1$ value was determined at each investigated frequency by fitting the experimental data. The NMRD curves obtained at different temperatures in the I, N*, and Cr phases are reported in Figure 2.

In the I phase (Figure 2a) the $^1$H NMRD curves show a plateau in the low Larmor frequency region, covering a frequency range which gets smaller with decreasing the temperature. The $R_1$ values at the plateau vary with temperature, ranging from 20 to 150 $s^{-1}$ by cooling from 319 to 301 K. No clear dependence of $R_1$ on the square root of the Larmor frequency is observed in the low frequency limit (see Figure S1), indicating that translational diffusion does not give a dominant contribution. At all temperatures a steep decrease of $R_1$ is observed above $10^6$ Hz, while an additional relaxation contribution, ascribable to order fluctuations, is present only below 315 K. Indeed, the latter gives rise to a linear dependence of $R_1$ on the inverse of the square root of the Larmor frequency over a frequency region, the center of which moves from $10^7$ to $10^6$ Hz with decreasing the temperature (see Figure S2). At 300 K a change in the dispersion shape is observed, especially in the $10^4$−$10^6$ Hz frequency range, ascribable to the I to N* phase transition.

In the N* phase (Figure 2b), similar dispersion curves are observed at all temperatures from 300 to 283 K. The NMRD profiles are quite complex, showing the contributions of at least two motional processes, one below $10^5$ Hz and the other at about $10^7$ Hz. In particular, the trend of $R_1$ in the low frequency


DOI: 10.1021/acs.jpcb.6b03773
J. Phys. Chem. B 2016, 120, 5083−5092

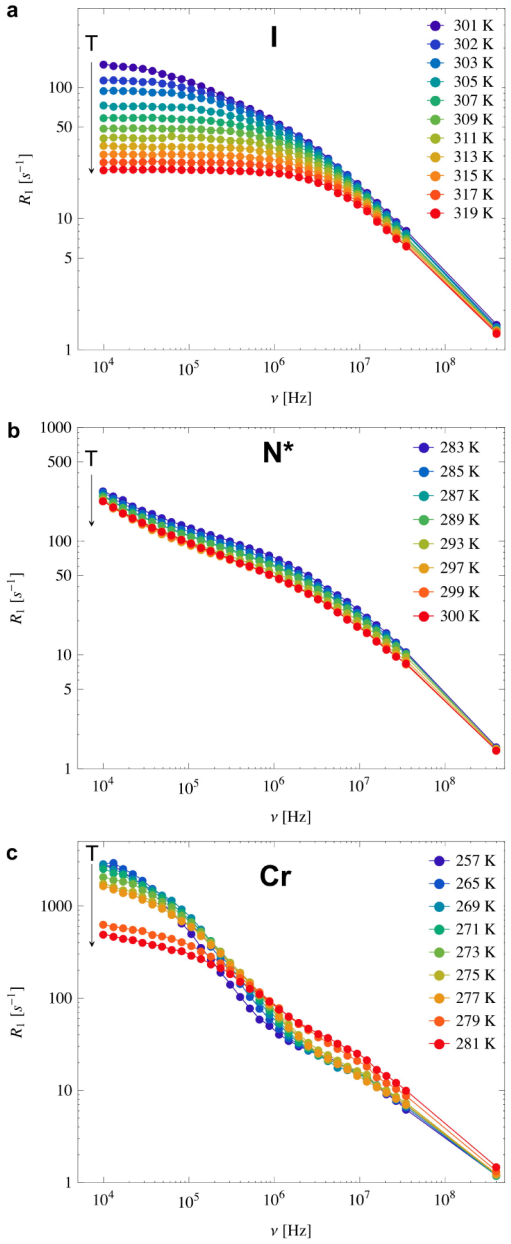


**Figure 2.** $^1$H spin−lattice relaxation rates as a function of Larmor frequency measured on 4ABO5* in the 257−319 K temperature range. Lines only serve to guide the eyes. In (c), data at 279 and 281 K are in the supercooled N* phase.

region (below 100 kHz) shows a linear dependence of $R_1$ on the inverse square root of the Larmor frequency, as highlighted in Figure 3 (see also Figure S3), typical of ODF in N and N* phases.[24,25]

In the Cr phase (Figure 2c), the NMRD profiles show a contribution to $R_1$ in the $10^5$−$10^6$ Hz range; a second one starts to be visible at high frequencies, indicating the presence of a dynamic process with characteristic frequency higher than $10^7$ Hz. Features of the NMRD curves intermediate between those of N* and Cr phases are observed at 279 and 281 K, where a supercooled liquid crystalline phase, also observed by DSC (see Experimental section), is most probably present.

The largest differences among the I, N*, and Cr phases are observed in the low frequency region, where $R_1$ values are 20−180 $s^{-1}$, 200−500 $s^{-1}$, and >1000 $s^{-1}$, respectively. On the

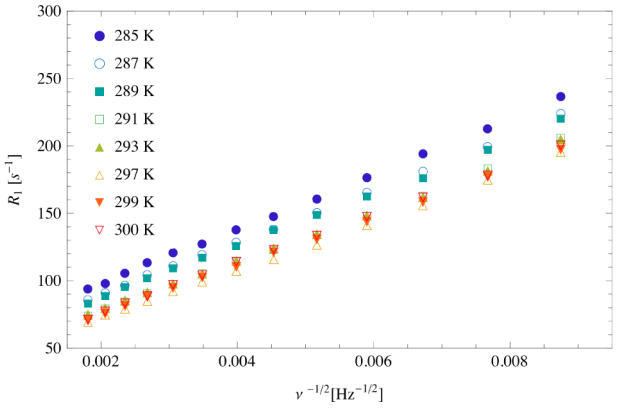


**Figure 3.** Trends of $^1$H $R_1$ values as a function of the inverse square root of the Larmor frequency at the indicated temperatures in the N* phase.

contrary, at the highest investigated frequency (400 MHz), the $R_1$ values are quite similar in all phases, indicating the presence of a fast motion, with characteristic correlation time shorter than $10^{-10}$ s, at all temperatures.

The temperature dependence of $R_1$ in the different phases is shown in Figure 4 for selected Larmor frequencies. Within the I

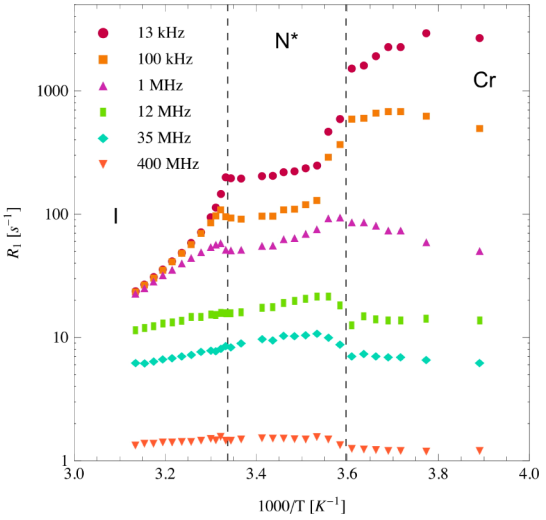


**Figure 4.** Temperature dependence of $R_1$ at the indicated $^1$H Larmor frequencies. Vertical dashed lines correspond to the phase transition temperatures determined by DSC on cooling.[29]

and N* phases, the $R_1$ values increase by decreasing the temperature at all Larmor frequencies; however, while at higher frequencies a similar dependence is maintained when passing from the I to the N* phase, for the lower frequencies ($\lesssim$ 1 MHz) an abrupt change of the slope is observed at the phase transition. This behavior seems to indicate that the motion(s) dominating the longitudinal relaxation at high frequency is minimally affected by the onset of the ordered phase. Moreover, the slope of $R_1$ vs 1000/$T$ increases by decreasing the frequency in the I phase, while it remains quite similar in the N* one. This behavior suggests that a second relaxation mechanism, efficient in the intermediate to low frequencies, is present in the isotropic phase with a contribution to the relaxation rate that increases on cooling as the I to N* phase transition temperature is approached. A similar trend was previously observed for a cholesteric liquid crystal and ascribed



DOI: 10.1021/acs.jpcb.6b03773
J. Phys. Chem. B 2016, 120, 5083−5092

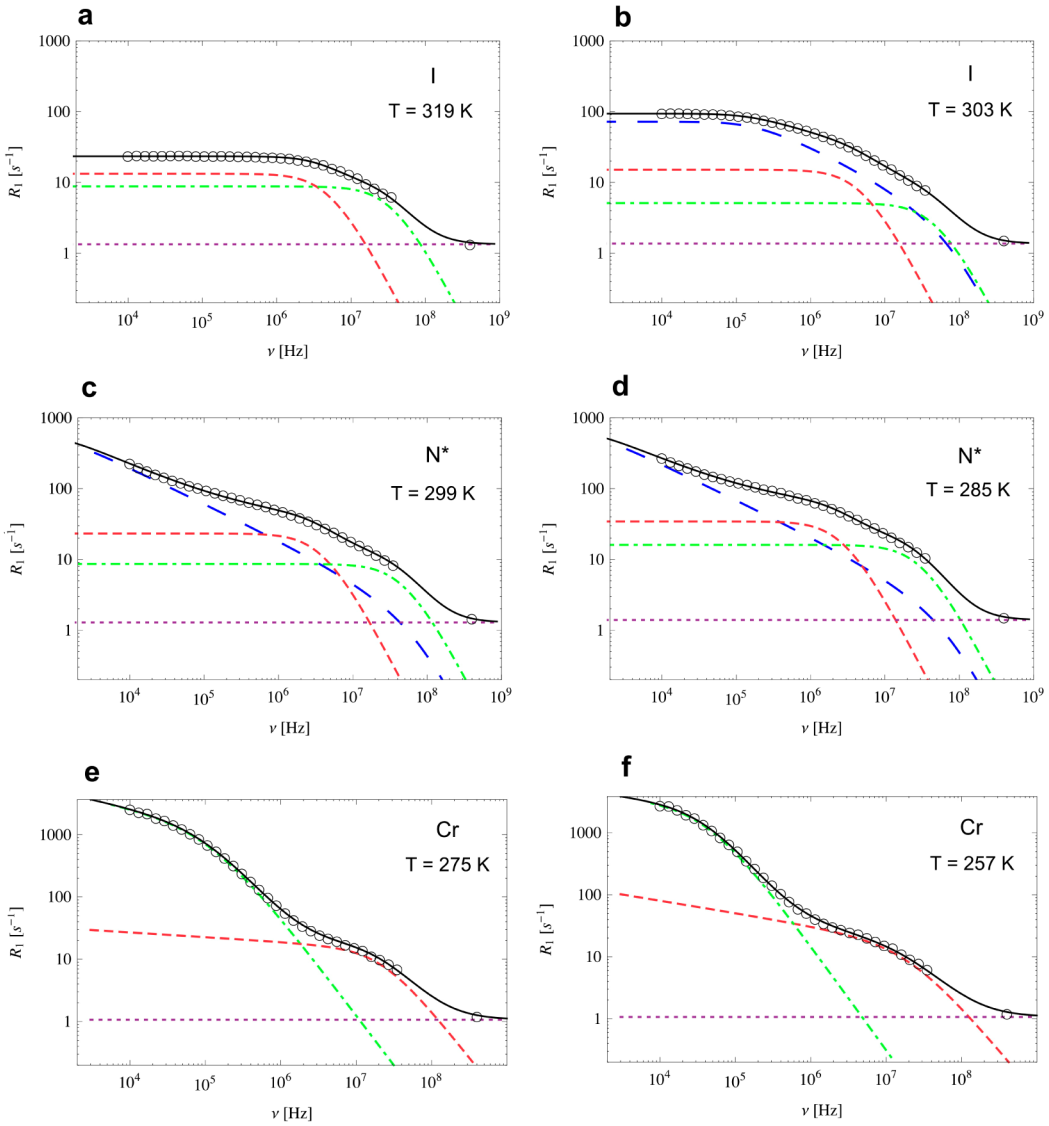


**Figure 5.** Experimental (circles) and calculated (black lines) $^1$H relaxation rates in the I (a,b), N* (c,d) and Cr (e,f) phases of 4ABO5* at some selected temperatures. Red-dashed and green dot-dashed lines indicate L and S reorientational contributions, respectively; purple-dotted lines indicate the frequency-independent I contribution; blue long-dashed lines indicate the collective motions contribution (ODF for the N* phase and OF for the I phase).

to pretransitional order fluctuation effects.[26] The presence of an OF contribution is here confirmed by the linear dependence of $R_1$ on the inverse square root of the Larmor frequency observed in a frequency region that shifts to lower frequencies by decreasing the temperature in the I phase (Figure S2). On the other hand, the trends observed in Figure 4 for the N* phase confirm that the same relaxation processes contribute to relaxation at all temperatures down to 283 K in this phase. On cooling from the N* to the Cr phase, the trends of $R_1$ support the occurrence of a mesophase supercooling at 279 and 281 K. In the Cr phase, $R_1$ values show different temperature dependences at different frequencies.

**Analysis of NMRD Curves.** The analysis of the acquired NMRD curves is not straightforward and, if we take into account all the different kinds of molecular (reorientations (MR), self-diffusion (SD), and molecular rotations induced by translational diffusion (RMTD)), collective (OF or ODF), and internal motions (IM) that may in principle contribute to the observed relaxation rates, several different combinations could give a comparably good reproduction of the experimental data. The analysis was therefore performed in each phase considering the different motions that could be present on the basis of peculiar features in the NMRD curves (Figures 2, 3, S1−S3) or in the trends of $R_1$ with temperature (Figure 4), and following the criterion of using the minimum number of contributions to $R_1$ that well reproduce the experimental trends with physically reasonable parameter values in order to avoid overinterpretation of data. Fitting procedures minimizing the least-squares of residuals between experimental and calculated data were applied to all NMRD curves (see Experimental section) considering the models described below.

In the I phase, for temperatures higher than 313 K, the experimental NMRD curves could be well-reproduced considering a contribution ($C_I$) which is independent of frequency over the investigated range and two rotational diffusion contributions, each described with the BPP model (eqs 2 and 3), characterized by correlation times on the order of $10^{-8}$ and $10^{-9}$ s; an example is shown in Figure 5a. It must



DOI: 10.1021/acs.jpcb.6b03773
J. Phys. Chem. B 2016, 120, 5083−5092

be pointed out that a good reproduction of the NMRD curves could also be obtained by considering a translational diffusion contribution to $R_1$, expressed using the Torrey model,[36] either in place of or in addition to the rotational contribution at intermediate frequency. Although translational diffusion is often considered as a relaxation mechanism in the interpretation of NMRD curves in N and N* phases,[7,11,19−21,25,44] our data do not allow the contribution of this motion to be unambiguously distinguished from that of the rotational motion at the intermediate frequency, which is indeed shown to be present by BDS data.[28] The situation is further complicated for the NMRD curves at the lower temperatures in the I phase and in the N* phase, where OF and ODF contributions are also respectively present. This considered, we preferred to keep the fitting model as simple as possible to avoid data over-interpretation; therefore, the lowest number of contributions, with the simplest spectral densities and requiring the minimum number of fitting parameters, were considered in the analysis. With this choice, also taking into account the trend of $R_1$ at high frequency in the whole temperature range investigated (Figures 2 and 4), the $C_I$ contribution can be ascribed to internal motions, most probably methyl or phenyl ring rotations with correlation times shorter than $10^{-10}$ s. On the other hand, considering the findings of BDS previously reported for 4ABO5*,[28] the BPP contributions can be assigned to molecular motions, that is to rotations around the long (L motion) and short molecular axes (S motion). At temperatures lower than 313 K, an additional contribution arising from local order fluctuations connected with pretransitional effects, $R_1^{OF}$ expressed as in eq 4, was also required to fit the experimental data (for example, see Figure 5b). Very good reproductions of NMRD curves were obtained with the correlation time values shown in Figure 6 and the best fit parameters reported in Table 1. In particular, $C_{OF}$ and $\omega_0/2\pi$ ranged from $1 \times 10^4$ to $4 \times 10^4$ $s^{-3/2}$ and from $32 \times 10^4$ to $4 \times 10^4$ Hz, respectively, on decreasing the temperature from 313 to 301 K. On the other hand, the high-frequency and low-frequency cutoff values were $\omega_{OFmax}/2\pi = 10^8$ Hz and $\omega_{OFmin}/2\pi \leq 10^4$ Hz, respectively, at all the temperatures. The correlation time of the S motion, $\tau_S$, slightly increased by decreasing the temperature, whereas only a high limit value, almost constant over the whole temperature range, could be determined for the correlation time, $\tau_L$, of the L motion.

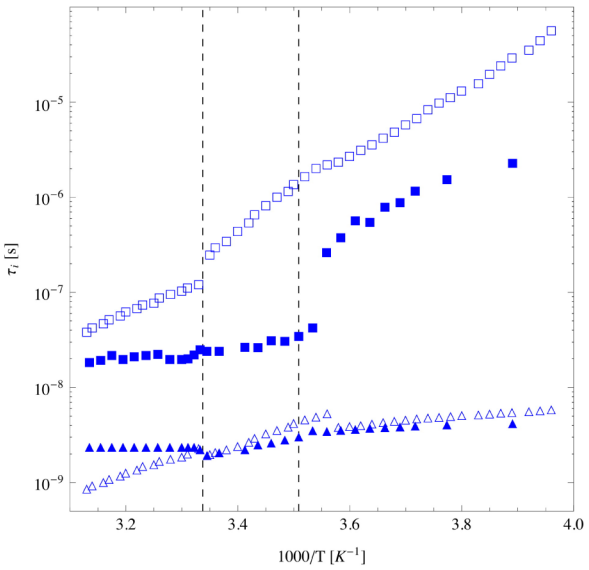


**Figure 6.** Trend of correlation times $\tau_S$ (squares) and $\tau_L$ (triangles) vs 1000/$T$. Correlation times determined by $^1$H FFC NMR and BDS have full and empty symbols, respectively. Vertical dashed lines correspond to the phase transition temperatures determined by DSC on cooling.[29] BDS data are taken from ref 28.

In the N* phase, at all the investigated temperatures, the NMRD curves could be well-reproduced (examples are shown in Figure 5c,d), considering a contribution independent of frequency ($C_I$) and two molecular reorientation contributions modeled using the BPP function (eq 3), as in the isotropic phase, plus a contribution arising from ODF motions, modeled using eq 5. The choice of the BPP model for molecular reorientations also in the N* phase, adopted also by other authors in chiral phases,[20,21] was dictated by the lack of knowledge of the geometrical and orientational order parameters required by more complex models, as well as by the complexity of the system, where the measured $R_1$ arises from different pairs of protons and different molecular orientations with respect to the external magnetic field (see Theoretical Background section). The fitting parameters were $C_{ODF}$, $\omega_{ODFmax}$, and $\omega_{ODFmin}$ for ODF and the correlation times ($\tau_S$ and $\tau_L$) and amplitude factors ($C_S$ and $C_L$) for S and L reorientational motions, respectively; the best-fit values are reported in Figure 6 and Table 1. A high-frequency cutoff value of $\omega_{ODFmax}/2\pi = 10^8$ Hz was found by fitting the experimental data, whereas for $\omega_{ODFmin}$, a limit value of $5 \times 10^3$ Hz was estimated. The best-fitting values of $C_{ODF}$ determined in the N* phase ranged from $2.0 \times 10^4$ to $2.2 \times 10^4$ $s^{-3/2}$ by decreasing the temperature, in agreement with the dependence of $C_{ODF}$ on temperature and on the principal order parameter. $\tau_L$ and $\tau_S$ increased by decreasing the temperature with associated activation energies, determined by the Arrhenius equation, equal to 21 ± 3 kJ/mol for both motions.

In the Cr phase, two molecular reorientation processes (S and L, with $\tau_S > \tau_L$) had to be considered, both modeled using the HN spectral densities (eq 7) and $C_i$, $\tau_i$, $\beta_i$, $\delta_i$ (with i = L or S) as fitting parameters for the $i$-th motion, in addition to a constant contribution ($C_I$). A very good reproduction of the NMRD data was obtained at all temperatures; examples are shown in Figure 5e,f, and the best fit parameters are reported in Figure 6 and Table 1. As shown in the figure, although the S motion has been described with different spectral density models in the N* and Cr phases (BPP and HN, respectively), we can safely affirm that it substantially slows down upon entering the Cr phase. Moreover, a stronger dependence of $\tau_S$ on temperature is observed in the Cr phase with respect to the fluid phases; an activation energy of 47 ± 5 kJ/mol could be estimated assuming an Arrhenius-type dependence. These findings suggested a change in the mechanism of the molecular reorientations about the short axis.

Finally, a slightly increasing trend of $C_S$ and $C_L$ is observed on going from the I to the N* and Cr phases, which is consistent with the decreasing overall mobility.

**Comparison between NMR Relaxometry and Dielectric Spectroscopy.** In Figure 6, the correlation times here determined in the analysis of $^1$H NMR relaxometry data are compared to those obtained in a previous work by BDS.[28] It must be reminded that BDS data were analyzed in terms of the HN model (eq 7) for all motions in all phases. The largest differences were observed for the S motion in the N* phase where, however, a larger uncertainty is present in the data


DOI: 10.1021/acs.jpcb.6b03773
J. Phys. Chem. B 2016, 120, 5083−5092

Table 1. Parameters Obtained by Fitting the NMRD Curves to Model Spectral Densities As Described in the Text[a]

| | phase | | |
|---|---|---|---|
| parameter | I | N* | Cr |
| $C_I$ ($s^{-1}$) | 1.3 ± 0.1 | 1.3 ± 0.1 | 1.1 ± 0.2 |
| $C_S$ ($s^{-2}$) | (1.7 ± 0.2) × $10^8$ | (1.9 ± 0.2) × $10^8$ | (2.0 ± 0.5) × $10^8$ |
| $C_L$ ($s^{-2}$) | (6 ± 1) × $10^8$ | (9 ± 1) × $10^8$ | (9 ± 1) × $10^8$ |
| $\beta_S$ | - | - | 0.8 |
| $\beta_L$ | - | - | 0.6 |
| $\delta_S$ | - | - | 0.8−0.9 |
| $\delta_L$ | - | - | 0.7−0.9 |
| $C_c$ ($s^{-3/2}$) | (1−4) × $10^4$ | (2.0−2.2) × $10^4$ | - |
| $\omega_0/2\pi$ (Hz) | (4−32) × $10^4$ | - | - |
| $\omega_{cmin}/2\pi$ (Hz) | ≤$10^4$ | ≤5 × $10^3$ | - |
| $\omega_{cmax}/2\pi$ (Hz) | $10^8$ | $10^8$ | - |

[a]Index c refers to collective motions, that is OF and ODF in the I and N* phases, respectively.

analysis for both methods, due to the superposition of different contributions to relaxation. In particular, in the analysis of $^1$H NMRD curves, a heavy superposition is found between the $R_1$ contributions arising from the S motion and the ODF collective fluctuations.

In the Cr phase, where the HN model was used to analyze relaxation arising from S and L motions for both methods, a more direct comparison between BDS and NMR data could be made exploiting the susceptibility representation. In Figure 7,

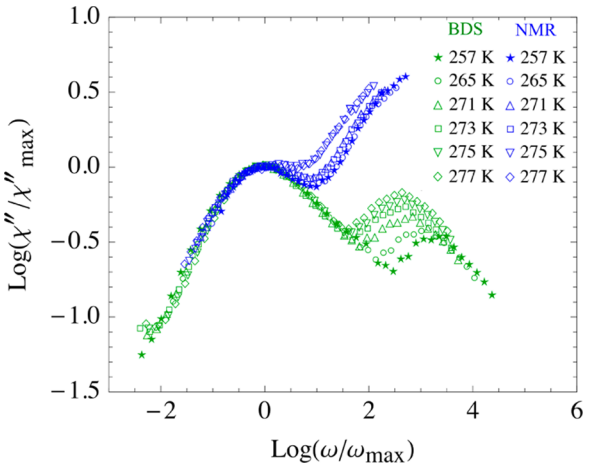


**Figure 7.** Master curve built with $\chi''_{NMR}(\omega)$ and $\chi''_{BDS}(\omega)$ scaled data at the indicated temperatures. The horizontal axis is defined as $\log(\omega/\omega_{max})$, where $\omega_{max}$ is the frequency of the maximum value of $\chi''_{NMR}(\omega)$ or $\chi''_{BDS}(\omega)$ for the reorientation around the short molecular axis (S motion), and the vertical axis is defined as $\log(\chi''_{NMR}/\chi''_{NMR,max})$ and $\log(\chi''_{BDS}/\chi''_{BDS,max})$ for NMR (blue symbols) and BDS (green symbols) data, respectively. $\chi''_{BDS}(\omega)$ data are taken from ref 28.

master curves built with data acquired between 257 and 277 K are reported: the horizontal axis was defined for both methods as $\log(\omega/\omega_{max})$, where $\omega_{max}$ is the frequency of the maximum value of $\chi''_{NMR}(\omega)$ or $\chi''_{BDS}(\omega)$ for the reorientation around the short molecular axis (S motion), and the vertical axis was defined as $\log(\chi''_{NMR}/\chi''_{NMR,max})$ and $\log(\chi''_{BDS}/\chi''_{BDS,max})$ for NMR and BDS data, respectively.

The obtained master curves indicate that both $\chi''_{NMR}(\omega)$ and $\chi''_{BDS}(\omega)$ data are in agreement with FTS. Moreover, NMR and BDS scaled data lie exactly on the same curve for frequencies lower than $\omega_{max}$ and temperatures between 265 and 273 K; for 275 K, small discrepancies could be noticed only for very low frequencies. At 257 and 277 K, larger differences were observed, with the scaled NMR and BDS data lying on one master-curve only in the vicinity of the maximum. On the other hand, the scaled NMR and BDS curves diverge at frequencies higher than $\omega_{max}$, where the relaxation process associated with reorientations around the long molecular axis shows up.

The $\tau_S$ values determined by fitting the NMR and BDS data in the Cr phase using the HN spectral density with quite similar $\delta$ and $\beta$ parameters (Table 1 and ref 28) are compared in Figure 6. The correlation times obtained from the BDS method are 4−6 times higher, indicating that, if all the distinctions pointed out in the Theoretical Background section are considered, the agreement between NMR and BDS data can be judged quite good. Indeed, a factor of 3 is theoretically expected between BDS and NMR correlation times for rotational diffusion, and experimental ratios close to 3 are reported in the literature.[49,50,52,53]

## CONCLUSIONS

In this work, we presented a comprehensive study of the molecular dynamics in the isotropic liquid, cholesteric, and crystalline phases of a chiral liquid crystal, 4ABO5*. The $^1$H relaxation rates were measured over a broad frequency range (from 10 kHz to 400 MHz), and their temperature dependence was investigated in all phases.

A thorough analysis of NMRD curves was performed using models that take into account the relevant relaxation mechanisms in the different phases. In the I phase, overall reorientational motions were singled out at all the temperatures, whereas order fluctuations were clearly observed approaching the I to N* phase transition. Order director fluctuations dominated relaxation in the N* phase, where the molecular reorientational motions were still present. These molecular motions remained also in the Cr phase, although characterized by a broad distribution, as pointed out by the fact that the Havriliak−Negami model was necessary instead of the Bloembergen−Purcell−Pound one to describe the spectral densities. A contribution of translational diffusion to relaxation in the I and N* phases cannot be excluded, but the experimental data do not allow it to be clearly distinguished. On the basis of the correlation time values and their trend with temperature, the reorientational motion about the long molecular axis can be identified as rotational diffusion in all phases, whereas the motion about the short molecular axis is most probably a rotational diffusion in the I and N* phases and a small amplitude reorientation in the Cr phase.



DOI: 10.1021/acs.jpcb.6b03773
J. Phys. Chem. B 2016, 120, 5083−5092

The NMR relaxometry data were also compared to BDS data previously obtained on the same compound in the three phases. To this aim, the susceptibility representation was used for the NMR data in the crystalline phase. Notwithstanding the highlighted differences between the two methods, the findings corroborate the interpretation of the experimental data in terms of dynamic processes.

## ■ ASSOCIATED CONTENT

### Supporting Information

The Supporting Information is available free of charge on the ACS Publications website at DOI: 10.1021/acs.jpcb.6b03773.

Trends of $R_1$ vs the square root of Larmor frequency in the I phase. Trends of $R_1$ vs the inverse square root of Larmor frequency in the I and N* phases. (PDF)

## ■ AUTHOR INFORMATION


### Corresponding Authors

*E-mail: lucia.calucci@pi.iccom.cnr.it. Phone: +39-050-3152517. Fax: +39-050-3152555.

*E-mail: marco.geppi@unipi.it. Phone: +39050-2219289. Fax: +39-0502219260.


### Author Contributions

The manuscript was written through contributions of all authors. All authors have given approval to the final version of the manuscript.

### Notes

The authors declare no competing financial interest.

## ■ ACKNOWLEDGMENTS

This work was supported by the 2014-2016 CNR-PAS bilateral project "Studies of phase polymorphism and dynamics in selected soft materials".

## ■ ABBREVIATIONS

4ABO5*:4′-butyl-4-(S)-(2-methylbutoxy)azoxybenzene; FFC:Fast Field-Cycling; BDS:broadband dielectric spectroscopy; NMRD:nuclear magnetic relaxation dispersion; ODF:order director fluctuations; OF:order fluctuations; SD:self-diffusion; IM:internal motions; CM:collective motions; MR:molecular reorientations; RMTD:rotation mediated by translational diffusion; FTS:frequency temperature superposition

## ■ REFERENCES


(1) Chandrasekhar, S. *Liquid Crystals*; Cambridge University Press: Cambridge, 1977.

(2) *Handbook of Liquid Crystals*; Demus, D., Goodby, J., Gray, G. W., Spiess, H. W., Vill, V., Eds.; Wiley-VCH: Weinheim, 1998.

(3) *Relaxation Phenomena*; Haase, W., Wróbel, S., Eds.; Springer-Verlag: Berlin, 2003.

(4) Fisch, M. R. *Liquid Crystals. Laptops and Life*; World Scientific Publishing Co. Pte. Ltd: Singapore, 2004.

(5) *The Molecular Dynamics of Liquid Crystals*; Luckhurst, G. R., Veracini, C. A., Eds.; Kluwer Academic: Dordrecht, 1994.

(6) Dong, R. Y. *Nuclear Magnetic Resonance of Liquid Crystals*; Springer: New York, 1997.

(7) *Nuclear Magnetic Resonance Spectroscopy of Liquid Crystals*; Dong, R. Y., Ed.; World Scientific: Singapore, 2010.

(8) Domenici, V.; Geppi, M.; Veracini, C. A. NMR in Chiral and Achiral Smectic Phases: Structure, Orientational Order and Dynamics. *Prog. Nucl. Magn. Reson. Spectrosc.* **2007**, *50*, 1−50.

(9) *Nuclear Magnetic Resonance of Liquid Crystals*; Emsley, J. W., Ed.; Reidel: Dordrecht, 1985; Chapter 9, pp 207−230.

(10) Kremer, F.; Schönhals, A. *Molecular and Collective Dynamics of (Polymeric) Liquid Crystals in Broadband Dielectric Spectroscopy*; Springer-Verlag: Berlin, 2003.

(11) Noack, F. NMR Field-Cycling Spectroscopy: Principles and Applications. *Prog. Nucl. Magn. Reson. Spectrosc.* **1986**, *18*, 171−276.

(12) Dong, R. Y. Relaxation and the Dynamics of Molecules in the Liquid Crystalline Phases. *Prog. Nucl. Magn. Reson. Spectrosc.* **2002**, *41*, 115−151.

(13) Dong, R. Y. Spin Relaxation in Orientationally Ordered Molecules. In *NMR of Ordered Liquids*; Burnell, E. E., de Lange, C. A., Eds.; Kluwer Academic: Dordrecht, 2003; Chapter 16, pp 349−373.

(14) Kruk, D.; Herrmann, A.; Rossler, E. A. Field-Cycling NMR Relaxometry: of Viscous Liquids and Polymers. *Prog. Nucl. Magn. Reson. Spectrosc.* **2012**, *63*, 33−64.

(15) Meier, R.; Kruk, D.; Bourdick, A.; Schneider, E.; Rössler, E. A. Inter- and Intramolecular Relaxation in Molecular Liquids by Field Cycling $^1$H NMR Relaxometry. *Appl. Magn. Reson.* **2013**, *44*, 153−168.

(16) Fujara, F.; Kruk, D.; Privalov, A. F. Solid State Field-Cycling NMR Relaxometry: Instrumental Improvements and New Applications. *Prog. Nucl. Magn. Reson. Spectrosc.* **2014**, *82*, 39−69.

(17) Sousa, D. M.; Marques, G. D.; Sebastião, P. J.; Ribeiro, A. C. New Isolated Gate Bipolar Transistor Two-Quadrant Chopper Power Supply for a Fast Field Cycling Nuclear Magnetic Resonance Spectrometer. *Rev. Sci. Instrum.* **2003**, *74*, 4521−4528.

(18) Kimmich, R.; Anoardo, E. Field-Cycling NMR Relaxometry. *Prog. Nucl. Magn. Reson. Spectrosc.* **2004**, *44*, 257−320.

(19) Sebastião, P. J.; Gradišek, A.; Pinto, L. F. V.; Apih, T.; Godinho, M. H.; Vilfan, M. Fast Field-Cycling NMR Relaxometry Study of Chiral and Nonchiral Liquid Crystals. *J. Phys. Chem. B* **2011**, *115*, 14348−14358.

(20) Apih, T.; Domenici, V.; Gradišek, A.; Hamplová, V.; Kaspar, M.; Sebastião, P. J.; Vilfan, M. $^1$H NMR Relaxometry Study of a Rod-Like Chiral Liquid Crystal in Its Isotropic, Cholesteric, TGBA*, and TGBC* phases. *J. Phys. Chem. B* **2010**, *114*, 11993−12001.

(21) Gradišek, A.; Apih, T.; Domenici, V.; Novotna, V.; Sebastião, P. J. Molecular Dynamics in a Blue Phase Liquid Crystal: a $^1$H Fast Field-Cycling NMR Relaxometry Study. *Soft Matter* **2013**, *9*, 10746−10753.

(22) Grinberg, F.; Vilfan, M.; Anoardo, E. Low-Frequency NMR Relaxometry of Spatially Constrained Liquid Crystals. In *NMR of Ordered Liquids*; Burnell, E. E., de Lange, C. A., Eds.; Kluwer Academic: Dordrecht, 2003; Chapter 17, pp 375−398.

(23) Abragam, A. *The Principles of Nuclear Magnetism*; Clarendon Press: Oxford, 1961.

(24) Wölfel, W.; Noack, F.; Stohrer, M. Frequency Dependence of Proton Spin Relaxation in Liquid Crystalline PAA. *Z. Naturforsch., A: Phys. Sci.* **1975**, *30*, 437−441.

(25) Noack, F.; Notter, M.; Weiss, W. Relaxation Dispersion and Zero-Field Spectroscopy of Thermotropic and Lyotropic Liquid Crystals by Fast Field-Cycling NMR. *Liq. Cryst.* **1988**, *3*, 907−925.

(26) Vilfan, M.; Blinc, R.; Dolinšek, J.; Ipavec, M.; Lahajnar, G.; Žumer, S. Dispersion of Proton Spin-Lattice Relaxation in a Cholesteric Liquid Crystal. *J. Phys. (Paris)* **1983**, *44*, 1179−1184.

(27) Brás, A. R.; Dionísio, M.; Huth, H.; Schick, Ch.; Schönhals, A. Origin of Glassy Dynamics in a Liquid Crystal Studied by Broadband Dielectric and Specific Heat Spectroscopy. *Phys. Rev. E* **2007**, *75*, 061708.

(28) Juszyńska-Gałązka, E.; Gałązka, M.; Massalska-Arodź, M.; Bąk, A.; Chłędowska, K.; Tomczyk, W. Phase Behavior and Dynamics of the Liquid Crystal 4′-butyl-4-(2-methylbutoxy)azoxybenzene (4ABO5*). *J. Phys. Chem. B* **2014**, *118*, 14982−14989.

(29) Roy, D.; Fragiadakis, D.; Roland, C. M.; Dąbrowski, R.; Dziaduszek, J.; Urban, S. Phase Behavior and Dynamics of a Cholesteric Liquid Crystal. *J. Chem. Phys.* **2014**, *140*, 074502.

(30) Anoardo, E.; Galli, G.; Ferrante, G. Fast-Field-Cycling NMR: Applications and Instrumentation. *Appl. Magn. Reson.* **2001**, *20*, 365−404.

(31) Sebastião, P. J. Fitteia. Fitting Environment Interfaces for All. http://fitteia.org (date last accessed: May 11, 2016).

(32) Sebastião, P. J. The Art of Model Fitting to Experimental Results. *Eur. J. Phys.* **2014**, *35*, 015017.
(33) *Mathematica*, version 10.1.0.0, 2015; Trademark of Wolfram Research Inc: Champaign, IL, 2016.
(34) Redfield, A. G. The Theory of Relaxation Processes. In *Advances in Magnetic Resonance*; Waugh, J. S., Ed; Academic Press: New York, 1965; Vol. *1*, pp 1−32.
(35) Bloembergen, N.; Purcell, E. M.; Pound, R. V. Relaxation Effects in Nuclear Magnetic Resonance Absorption. *Phys. Rev.* **1948**, *73*, 679−712.
(36) Torrey, H. C. Nuclear Spin Relaxation by Translational Diffusion. *Phys. Rev.* **1953**, *92*, 962−969.
(37) Harmon, F.; Muller, B. N. Nuclear Spin Relaxation by Translational Diffusion in Liquid Ethane. *Phys. Rev.* **1969**, *182*, 400−409.
(38) Žumer, S.; Vilfan, M. Theory of Nuclear Spin Relaxation by Transational Self-Diffusion in Liquid Crystals: Nematic Phase. *Phys. Rev. A: At., Mol., Opt. Phys.* **1978**, *17*, 424−433.
(39) Belorizky, E.; Fries, P. H. Translational Diffusion in Liquids: Specific Features of the Spectral Densities for Isotropic Intermolecular Interactions. *Chem. Phys. Lett.* **1988**, *145*, 33−38.
(40) Sebastião, P. J.; Godinho, M. H.; Ribeiro, A. C.; Guillon, D.; Vilfan, M. NMR Study of Molecular Dynamics in a Mixture of Two Polar Liquid Crystals (CBOOA and DOBCA). *Liq. Cryst.* **1992**, *11*, 621−635.
(41) Vilfan, M.; Apih, T.; Sebastião, P. J.; Lahajnar, G.; Zumer, S. Liquid Crystal 8CB in Random Porous Glass: NMR Relaxometry Study of Molecular Diffusion and Director Fluctuations. *Phys. Rev. E* **2007**, *76*, 051708.
(42) Vilfan, M.; Žumer, S. Theory of Nuclear-Spin Relaxation by Translational Self-Diffusion in Liquid Crystals: Smectic A phase. *Phys. Rev. A: At., Mol., Opt. Phys.* **1980**, *21*, 672−680.
(43) Pincus, P. Nuclear Relaxation in a Nematic Liquid Crystal. *Solid State Commun.* **1969**, *7*, 415−417.
(44) Sebastião, P. J.; Ribeiro, A. C.; Nguyen, H. T.; Noack, F. Proton NMR Relaxation Study of Molecular Motions in a Liquid Crystal with a Strong Polar Terminal Group. *Z. Naturforsch., A: Phys. Sci.* **1993**, *48*, 851−860.
(45) Beckmann, P. A. Spectral Densities and Nuclear Spin Relaxation in Solids. *Phys. Rep.* **1988**, *171*, 85−128.
(46) Havriliak, S.; Negami, S. A Complex Plane Analysis of A-Dispersions in Some Polymer Systems. *J. Polym. Sci., Part C: Polym. Symp.* **1966**, *14*, 99−117.
(47) Böttcher, C. I. F.; Bordewijk, P. *Theory of Electric Polarization*; Elsevier: Amsterdam, 1978; Vol. *2*.
(48) Gałązka, M.; Juszyńska-Gałązka, E.; Osiecka, N.; Massalska-Arodź, M.; Bąk, A. On New Scaling of Dielectric Response. *J. Appl. Phys.* **2015**, *118*, 064101.
(49) Blochowicz, T.; Kudlik, A.; Benkhof, S.; Senker, J.; Rössler, E.; Hinze, G. The Spectral Density in Simple Organic Glass Formers: Comparison of Dielectric and Spin-Lattice Relaxation. *J. Chem. Phys.* **1999**, *110*, 12011−12022.
(50) Meier, R.; Kahlau, R.; Kruk, D.; Rössler, E. A. Comparative Studies of the Dynamics in Viscous Liquids by Means of Dielectric and Field-Cycling NMR. *J. Phys. Chem. A* **2010**, *114*, 7847−7855.
(51) Meier, R.; Kruk, D.; Rössler, E. A. Intermolecular Spin Relaxation and Translation Diffusion in Liquids and Polymer Melts: Insight from Field-Cycling $^{1}$H NMR Relaxometry. *ChemPhysChem* **2013**, *14*, 3071−3081.
(52) Kahlau, R. Primary and Secondary Relaxations in Neat and Binary Glass Formers Studied by Means of Dielectric Spectroscopy. PhD Thesis. Universität Bayreuth, Bayreuth, Germany, 2014.
(53) Feldman, Y.; Puzenko, A.; Ryabov, Y. Dielectric Relaxation Phenomena in Complex Materials. In *Fractals, Diffusion and Relaxation in Disordered Complex Systems: Advances in Chemical Physics, Part A, Volume 133*; Kalmykov, Y., Coffey, W. T., Rice, S. A., Eds; John Wiley & Sons: Hoboken, NJ, **2006**.


DOI: 10.1021/acs.jpcb.6b03773
*J. Phys. Chem. B* 2016, 120, 5083−5092